

**NANOSCALE BASED Ti/AlN/Ti/SiO<sub>2</sub> MULTI-LAYER ABSORBER COATINGS FOR SOLAR THERMAL DEVICES**

**BELLO MUTAWALLI**

**UNIVERSITI SAINS MALAYSIA**

**2022**

**NANOSCALE BASED Ti/AlN/Ti/SiO<sub>2</sub> MULTI-LAYER ABSORBER COATINGS FOR SOLAR THERMAL DEVICES**

by

**BELLO MUTAWALLI**

**Thesis submitted in fulfilment of the requirements  
for the degree of  
Doctor of Philosophy**

**April 2022**

## ACKNOWLEDGEMENT

Alhamdulillah, all praises are due to Allah. First and foremost, I would like to thank Allah for giving me wisdom, good health, knowledge, strength, and guidance in accomplishing this research work. My sincere gratitude goes to my main supervisor, Dr Shanmugan Subramani for his scholarly and valuable guidance, suggestions, dedicated time, and support throughout the period of this study. Thank you once again Sir for making your door open for me every time, I needed help despite your tight schedule. My appreciation also goes to my co-supervisor Dr Mohd Marzaini Bin Mohd Rashid his valuable inputs and guidance towards the success of this research work. This work would have been almost impossible without the technical supports of staff in Thermal Management Research Lab (TMRL) and Nano-Optoelectronics Research and Technology Laboratory (NOR) school of Physics, Universiti Sains Malaysia. My profound gratitude also goes to my lab colleagues Sani, El-ladan, Vishnu, Muralidharan, Vignesh and Purnaraj for their kindness and understanding in sharing ideas and experience together throughout the period of this research. I would like to thank Federal College of Education, Yola for a study leave and TetFund Nigeria for sponsoring my PhD degree. My heartfelt gratitude and appreciation goes to my loving parents Mal. Bello Abba and Late Khadija Bello, sisters, brothers, siblings, and friends especially M. H Modiddo for their prayers and encouragement during the period of my PhD journey. My special and in-depth appreciation goes to my loving wife Hafsat Ahmad and my daughters Ashraf, Khadeeja, Fatima and Fa'iza for their patience, endurance, encouragement, and prayers for the success of this research. Finally, my special appreciation to a brother and mentor per excellence Professor Ahmed Hammawa Song, his wife, and his children at large. Thank you. **Mutawalli Bello**

## TABLE OF CONTENTS

<b>ACKNOWLEDGEMENT</b> .....	<b>ii</b>
<b>TABLE OF CONTENTS</b> .....	<b>iii</b>
<b>LIST OF TABLES</b> .....	<b>viii</b>
<b>LIST OF FIGURES</b> .....	<b>ix</b>
<b>LIST OF SYMBOLS</b> .....	<b>xvii</b>
<b>LIST OF ABBREVIATIONS</b> .....	<b>xix</b>
<b>LIST OF APPENDICES</b> .....	<b>xxi</b>
<b>ABSTRAK</b> .....	<b>xxii</b>
<b>ABSTRACT</b> .....	<b>xxiv</b>
<b>CHAPTER 1 INTRODUCTION</b> .....	<b>1</b>
1.1 Introduction to Solar Energy .....	1
1.2 Properties of AlN, SiO <sub>2</sub> and Ti.....	4
1.3 Selective Solar Absorber Coatings.....	5
1.4 Theoretical Background of Spectral Selectivity.....	6
1.5 Problem Statement .....	11
1.6 Objectives.....	12
1.7 Research Contribution.....	13
1.8 Thesis Outline .....	15
<b>CHAPTER 2 LITERATURE REVIEW</b> .....	<b>17</b>
2.1 Introduction .....	17
2.2 Different Designs of Spectrally Selective Absorber Coatings .....	17
2.2.1 Intrinsic absorber coatings .....	19
2.2.2 Multilayer coatings.....	21
2.2.3 Semiconductor coatings .....	23
2.2.4 Blackbody-like solar absorber coatings .....	24

2.2.5	Metal-dielectric composite coatings.....	24
2.2.6	Textured surface coatings.....	26
2.3	Overview of AlN Thin Film Growth Techniques .....	26
2.4	Overview of SiO <sub>2</sub> Thin Film Growth Techniques .....	28
2.5	Performance Improvement by Surface Modification.....	30
2.6	Nitride Based Solar Selective Absorber Coatings.....	31
2.7	Oxide Based Solar Selective Absorber Coatings. ....	36
2.8	Commercially Available Mid and High Temperature Solar Selective Absorber Coatings.....	43
<b>CHAPTER 3 METHODOLOGY.....</b>		<b>47</b>
3.1	Introduction .....	47
3.2	Substrate Selection .....	49
3.2.1	Substrate cutting, cleaning, and processing .....	49
3.2.2	Silicon substrate cleaning.....	50
3.3	Growth of SS <sub>M</sub> /Ti/AlN/Ti/SiO <sub>2</sub> Multilayer Absorber Coatings.....	51
3.4	Characterizations .....	53
3.4.1	UV-Vis-NIR measurement.....	54
3.4.2	Infrared reflectance measurement .....	55
3.4.3	Structural studies by-X-ray diffraction .....	56
3.4.4	Surface morphology analysis by-Field Emission Scanning Electron Microscopy .....	59
3.4.5	Surface roughness analysis by-Atomic Force Microscopy .....	60
3.5	Short/Long Term Thermal Stability.....	62
3.6	Durability Test.....	63
3.7	Adhesion Measurement.....	65
3.8	In-plane Thermal Analysis by-IR Imaging Camera .....	67

<b>CHAPTER 4</b>	<b>RESULTS AND DISCUSSION.....</b>	<b>69</b>
4.1	Synthesis and Optimization of Ti/AlN/Ti MSSAC on SS <sub>M</sub> Using Sputtering .....	69
4.1.1	Introduction .....	69
4.2	Effects of Substrate and Optimization of Ti <sub>BL</sub> .....	69
4.2.1	Optical properties of Ti <sub>BL</sub> deposited onto pristine and SS <sub>M</sub> substrates .....	70
4.2.2	Optical constants of refractive index ( <i>n</i> ) and extinction coefficient ( <i>k</i> ) of Ti <sub>BL</sub> deposited onto pristine and SS <sub>M</sub> substrate.....	76
4.2.3	Thickness verification of Ti <sub>BL</sub> .....	80
4.2.4	Surface morphology analysis of SS <sub>M</sub> /Ti .....	81
4.2.5	Surface roughness analysis of SS <sub>M</sub> /Ti.....	84
4.2.6	Structural analysis of SS <sub>M</sub> /Ti .....	86
4.3	Optimization of AlN Middle Layer on SS <sub>M</sub> /Ti .....	87
4.3.1	Optical constants of SS <sub>M</sub> /Ti/AlN stack .....	90
4.3.2	AlN thickness verification in SS <sub>M</sub> /Ti/AlN stack.....	91
4.3.3	Surface morphology analysis of SS <sub>M</sub> /Ti/AlN stack.....	93
4.3.4	Surface roughness analysis of SS <sub>M</sub> /Ti/AlN stack .....	95
4.3.5	Structural analysis of SS <sub>M</sub> /Ti/AlN stack .....	97
4.4	Optimization of Ti <sub>TL</sub> on Top of SS <sub>M</sub> /Ti/AlN Stack.....	98
4.4.1	Variation of optical constants of SS <sub>M</sub> /Ti/AlN/Ti MSSACs at various thickness of Ti <sub>TL</sub> .....	101
4.4.2	Ti <sub>TL</sub> thickness verification in Ti/AlN/Ti stack .....	102
4.4.3	Surface morphology analysis of SS <sub>M</sub> /Ti/AlN/Ti MSSACs at different thickness of Ti <sub>TL</sub> .....	103
4.4.4	Surface roughness analysis of SS <sub>M</sub> /Ti/AlN/Ti MSSACS at various thickness of Ti <sub>TL</sub> .....	105
4.5	Thermal Stability of SS <sub>M</sub> /Ti/AlN/Ti MSSACs in Air.....	107
4.5.1	Optical constants of the optimized SS <sub>M</sub> /Ti/AlN/Ti MSSACs.....	110

4.5.2	Surface morphology of SS <sub>M</sub> /Ti/AlN/Ti MSSACs annealed at different temperatures in air .....	111
4.5.3	Surface roughness analysis of SS <sub>M</sub> /Ti/AlN/Ti MSSACs at various annealing temperatures .....	112
4.5.4	Structural analysis of SS <sub>M</sub> /Ti/AlN/Ti MSSACs.....	114
<b>CHAPTER 5 OPTIMIZATION AND ANALYSIS OF SiO<sub>2</sub> ANTIREFLECTION LAYER ON SS<sub>M</sub>/Ti/AlN/Ti ABSORBER COATING USING RF SPUTTERING TECHNIQUE .....</b>		<b>118</b>
5.1	Introduction .....	118
5.2	Optimization of SiO <sub>2</sub> AR Layer on Top of SS <sub>M</sub> /Ti/AlN/Ti Stack .....	118
5.2.1	Optical properties of SS <sub>M</sub> /Ti/AlN/Ti/SiO <sub>2</sub> MSSACs .....	119
5.2.2	Optical constants analysis of SS <sub>M</sub> /Ti/AlN/Ti/SiO <sub>2</sub> MSSACs .....	123
5.2.3	SiO <sub>2</sub> AR thickness verification in Ti/AlN/Ti/SiO <sub>2</sub> stack.....	124
5.2.4	Surface morphology analysis of SS <sub>M</sub> /Ti/AlN/Ti/SiO <sub>2</sub> MSSACs .....	125
5.2.5	Compositional properties of SS <sub>M</sub> /Ti/AlN/Ti/SiO <sub>2</sub> MSSACs.....	127
5.2.6	Surface roughness analysis of SS <sub>M</sub> /Ti/AlN/Ti/SiO <sub>2</sub> MSSACs ....	129
5.2.7	Thermal stability of SS <sub>M</sub> /Ti/AlN/Ti/SiO <sub>2</sub> MSSACs in air.....	131
5.2.8	Surface morphology analysis of annealed SS <sub>M</sub> /Ti/AlN/Ti/SiO <sub>2</sub> MSSAC. ....	133
5.2.9	Surface roughness analysis of annealed SS <sub>M</sub> /Ti/AlN/Ti/SiO <sub>2</sub> MSSACs.....	135
5.2.10	Structural analysis of SS <sub>M</sub> /Ti/AlN/Ti/SiO <sub>2</sub> MSSACs annealed at different temperature .....	137
5.3	Comparative Study on the Optical and Structural Properties of SS <sub>M</sub> /Ti/AlN/Ti/SiO <sub>2</sub> and SS <sub>M</sub> /AlN/Ti/AlN/SiO <sub>2</sub> MSSACs.....	138
5.3.1	Optical properties and thermal stability of SS <sub>M</sub> /AlN/Ti/AlN/SiO <sub>2</sub> MSSACs.....	138
5.3.2	Surface morphology analysis of SS <sub>M</sub> /AlN/Ti/AlN/SiO <sub>2</sub> MSSACs.....	142
5.3.3	Surface roughness analysis of SS <sub>M</sub> /AlN/Ti/AlN/SiO <sub>2</sub> MSSACs .....	143

5.3.4	Structural analysis of $SS_M/AlN/Ti/AlN/SiO_2$ MSSACs annealed at different temperature.....	143
5.4	Durability test of the optimized $SS_M/Ti/AlN/Ti/SiO_2$ MSSACs.....	145
5.4.1	Optical properties of $SS_M/Ti/AlN/Ti/SiO_2$ MSSACs before and after durability test .....	145
5.4.2	Surface morphology analysis of $SS_M/Ti/AlN/Ti/SiO_2$ MSSACs before and after durability test .....	149
5.4.3	Surface roughness analysis of $SS_M/Ti/AlN/Ti/SiO_2$ MSSACs before and after durability test .....	151
5.5	Scratch Adhesion Test of $SS_M/Ti/AlN/Ti/SiO_2$ MSSACs .....	152
5.6	Thermal Infrared Imaging Analysis .....	157
<b>CHAPTER 6 CONCLUSION AND RECOMMENDATIONS .....</b>		<b>161</b>
6.1	Summary and Concluding Remarks.....	161
6.2	Recommendations for Future Work.....	163
<b>REFERENCES.....</b>		<b>165</b>
<b>APPENDICES</b>		
<b>LIST OF PUBLICATIONS</b>		
<b>LIST OF CONFERENCES</b>		

## LIST OF TABLES

	<b>Page</b>
Table 2.1	Summary of different configurations, optical properties, and thermal stability of some high temperature physical vapor deposited solar selective absorber coatings. ....40
Table 2.2	Commercially available mid and high temperature solar selective absorber coatings and their key properties.....46
Table 3.1	Sputtering process parameters for Ti/AlN/Ti/SiO <sub>2</sub> MSSAC.....52
Table 4.1	Effects of annealing temperature (400-600 °C) on the solar absorptance and thermal emittance of SS <sub>M</sub> /Ti/AlN/Ti MSSACs. ... 109
Table 4.2	Structural parameters for the SS <sub>M</sub> /Ti/AlN/Ti samples annealed at various temperatures in air for 2 h. .... 116
Table 5.1	Solar absorptance and thermal emittance alongside performance criterion of SS <sub>M</sub> /Ti/AlN/Ti/SiO <sub>2</sub> MSSACs after thermal shock and humidity tests. .... 148

## LIST OF FIGURES

		<b>Page</b>
Figure 1.1	World energy resources [5].....	2
Figure 1.2	Spectral selectivity of ideal absorber coating with reference AM 1.5G solar spectrum and ideal blackbody radiation at different temperatures [47]. .....	7
Figure 1.3	Spectrum of solar radiation [48]. .....	9
Figure 1.4	Schematic representation of cross-sectional view illustrating solar absorption and thermal IR emittance of: (a) uncoated and (b) coated steel pipes with solar selective absorber coating alongside (c) MDM coated pristine SS and (d) MDM coated SS <sub>M</sub> substrates. ....	14
Figure 2.1	Types of selective absorber surfaces.....	18
Figure 2.2	Schematic diagram of various types of solar absorber coatings (i) intrinsic absorber coating, (ii) multilayer coating, (iii) semiconductor coating, (iv) blackbody-like solar absorber coating, (v) metal-dielectric composite coating and (vi) textured surface coating. ....	18
Figure 2.3	Schematic representation of multilayer interference stack. ....	22
Figure 3.1	Comprehensive experimental flow chart. ....	48
Figure 3.2	(a) stainless steel and (b) silicon substrates.....	50
Figure 3.3	DC/RF magnetron sputtering machine (Model: AUTO 500). ....	51
Figure 3.4	Schematic stacking arrangement of Ti/AlN/Ti/SiO <sub>2</sub> MSSACs deposited onto SS <sub>M</sub> substrate. ....	53
Figure 3.5	Cary 5000 UV-Vis-NIR spectrophotometer. ....	54
Figure 3.6	Fourier transform infrared spectroscopy (FTIR).....	56
Figure 3.7	(a) Schematic representation of X-ray tube (b) Arrangement of atoms in a plane and the X-ray diffraction patterns. ....	58

Figure 3.8	PANalytical X'Pert PRO MRD PW3040 X-ray diffractometer. ....	59
Figure 3.9	Field Emission Scanning Electron Microscope. ....	60
Figure 3.10	Schematic representation of atomic microscope [198]. ....	61
Figure 3.11	Atomic Force Microscope (model: ULTRA Objectives Surface Imaging System, GmBh). ....	62
Figure 3.12	Single zone annealing furnace (model: GSL1100X, MTI Corp.). ....	63
Figure 3.13	(a) Compact thermal shock chamber and (b) Bench top-type temperature and humidity chamber. ....	65
Figure 3.14	(a) Taber shear/scratch tester, (b) schematic representation of scratch indenter. ....	66
Figure 3.15	Thermal infrared imaging experimental setup. ....	68
Figure 4.1	Reflectance spectra of various $Ti_{BL}$ thickness on pristine SS substrate. ....	71
Figure 4.2	Reflectance spectra of various thicknesses of $Ti_{BL}$ on $SS_M$ substrate. ....	72
Figure 4.3	IR reflectance spectra of various thicknesses of $Ti_{BL}$ deposited onto pristine SS substrates. ....	73
Figure 4.4	IR reflectance spectra of various thicknesses of $Ti_{BL}$ deposited onto $SS_M$ substrates. ....	74
Figure 4.5	Solar absorptance of $Ti_{BL}$ at different thicknesses deposited onto pristine and $SS_M$ substrates. ....	75
Figure 4.6	Thermal IR emittance of different $Ti_{BL}$ deposited onto pristine and $SS_M$ substrates. ....	76
Figure 4.7	(a) Refractive indices and (b) extinction coefficients of various thickness of $Ti_{BL}$ film deposited onto pristine SS substrate. ....	78
Figure 4.8	(a) Refractive indices and (b) extinction coefficients of various thickness of $Ti_{BL}$ deposited onto $SS_M$ substrate. ....	79
Figure 4.9	Summary of solar absorptance and thermal emittance values of $Ti_{BL}$ deposited onto pristine (P) and $SS_M$ (M) substrates. ....	80

Figure 4.10	Cross-sectional FESEM images of $Ti_{BL}$ coatings at: (a) 10 nm, (b) 15 nm, (c) 20 nm, (d) 25 nm, and (e) 30 nm Si substrate. ....	81
Figure 4.11	FESEM surface morphology of (a) pristine SS, (b) $SS_M$ and $SS_M/Ti$ coating at: (c) 10 nm, (d) 15 nm, (e) 20 nm, (f) 25 nm, and (g) 30 nm.....	83
Figure 4.12	Variation of grain size at different thickness of Ti on $SS_M$ .....	84
Figure 4.13	3D AFM images of: (a) reference $SS_M$ substrate and $SS_M/Ti$ at different thicknesses (b) 10 nm, (c) 15 nm, (d) 20 nm, (e) 25 nm, and (f) 30 nm.....	85
Figure 4.14	Plot of average surface roughness of a reference $SS_M$ substrate and the $Ti_{BL}$ thin film at different thicknesses. ....	86
Figure 4.15	XRD pattern of different thickness of $Ti_{BL}$ (a) 10 nm, (b) 15 nm, (c) 20 nm, (d) 25 nm, and (e) 30 nm deposited onto $SS_M$ substrates. ....	87
Figure 4.16	EDX spectra of $Ti_{BL}$ . ....	87
Figure 4.17	Reflectance spectra of $SS_M/Ti/AlN$ stack at various thickness of AlN.....	88
Figure 4.18	IR reflectance spectra of $SS_M/Ti/AlN$ stack at various AlN thicknesses. ....	90
Figure 4.19	Solar absorptance and thermal emittance of $SS_M/Ti/AlN$ stack at various AlN thickness. ....	90
Figure 4.20	Refractive index ( $n$ ) and extinction coefficient ( $k$ ) of $SS_M/Ti/AlN$ film at various AlN thickness.....	91
Figure 4.21	Cross-sectional FESEM images of Ti/AlN coatings at: (a) 15 nm, (b) 25 nm, (c) 35 nm, (d) 45 nm, and (e) 55 nm thickness of AlN deposited onto Si substrate.....	92
Figure 4.22	FESEM surface morphology of $SS_M/Ti/AlN$ coating at: (a) 15 nm, (b) 25 nm, (c) 35 nm, (d) 45 nm, and (e) 55 nm AlN thickness.....	94
Figure 4.23	Variation of grain size for various thickness of AlN in $SS_M/Ti/AlN$ stack.....	94

Figure 4.24	3D AFM images of SS <sub>M</sub> /Ti/AlN coating at: (a) 15 nm, (b) 25 nm, (c) 35 nm, (d) 45 nm, and (e) 55 nm AlN thickness. ....	96
Figure 4.25	Average surface roughness of SS <sub>M</sub> /Ti/AlN coating at different thickness of AlN.....	96
Figure 4.26	XRD pattern of SS <sub>M</sub> /Ti/AlN film at different thickness AlN (a) 15 nm, (b) 25 nm, (c) 35 nm, (d) 45 nm, and (e) 55 nm. ....	98
Figure 4.27	Variation in the intensity of (110) orientation with increase in AlN thickness.....	98
Figure 4.28	Reflectance spectra of SS <sub>M</sub> /Ti/AlN/Ti MSSACs at different thickness of Ti <sub>TL</sub> .....	99
Figure 4.29	IR reflectance spectra of SS <sub>M</sub> /Ti/AlN/Ti MSSACs at different thickness of Ti <sub>TL</sub> .....	101
Figure 4.30	Solar absorptance and thermal emittance of SS <sub>M</sub> /Ti/AlN/Ti MSSACs at different thickness of Ti <sub>TL</sub> .....	101
Figure 4.31	Optical constants of SS <sub>M</sub> /Ti/AlN/Ti MSSACs at different thickness of Ti <sub>TL</sub> .....	102
Figure 4.32	Cross-sectional FESEM images of Ti/AlN/Ti coatings at various thickness of Ti <sub>TL</sub> : (a) 5 nm, (b) 10 nm, (c) 15 nm, and (d) 20 nm deposited onto Si substrate.....	103
Figure 4.33	FESEM surface morphology of SS <sub>M</sub> /Ti/AlN/Ti MSSACs at different thickness of Ti <sub>TL</sub> : (a) 5 nm, (b) 10 nm, (c) 15 nm, and (d) 20 nm.....	104
Figure 4.34	Variation of grain size for various Ti <sub>TL</sub> in SS <sub>M</sub> /Ti/AlN/Ti stack. ....	105
Figure 4.35	3D AFM images of SS <sub>M</sub> /Ti/AlN/Ti coating at different thickness of Ti <sub>TL</sub> : (a) 5 nm, (b) 10 nm, (c) 15 nm, and (d) 20 nm. ....	106
Figure 4.36	Average surface roughness of SS <sub>M</sub> /Ti/AlN/Ti MSSACs at different thickness Ti <sub>TL</sub> . ....	106
Figure 4.37	Reflectance spectra of reference pristine and SS <sub>M</sub> , as-deposited SS <sub>M</sub> /Ti/AlN/Ti MSSACs and annealed at different temperatures in air for 2 h.....	108

Figure 4.38	IR reflectance spectra of reference pristine and $SS_M$ , as-deposited $SS_M/Ti/AlN/Ti$ MSSACs and annealed at different temperatures in air for 2 h. ....	109
Figure 4.39	Variation of $n$ and $k$ as a function of wavelength for the optimized $SS_M/Ti/AlN/Ti$ MSSACs. ....	110
Figure 4.40	FESEM micrographs of $SS_M/Ti/AlN/Ti$ MSSACs: (a) as-deposited, (b) annealed at 400 °C, (c) 500 °C, and (d) 600 °C in air for 2 h. ....	112
Figure 4.41	Variation of grain size with annealing temperature in air for $SS_M/Ti/AlN/Ti$ MSSACs. ....	112
Figure 4.42	3D AFM images of $SS_M/Ti/AlN/Ti$ MSSACs (a) as-deposited and annealed at (b) 400 °C, (c) 500 °C, and (d) 600 °C in air for 2 h. ....	113
Figure 4.43	Variation of mean surface roughness with annealing of $SS_M/Ti/AlN/Ti$ MSSACs. ....	114
Figure 4.44	XRD pattern of $SS_M/Ti/AlN/Ti$ tandem MSSACs (a) as-deposited and annealed at (b) 400 °C, (c) 500 °C, and (d) 600 °C in air for 2 h. ....	115
Figure 4.45	Variation in the intensity of (222) oriented peak with annealing temperature. ....	116
Figure 5.1	Reflectance spectra of $SS_M/Ti/AlN/Ti/SiO_2$ MSSACs at various thicknesses of $SiO_2$ AR layer. ....	121
Figure 5.2	IR reflectance of $SS_M/Ti/AlN/Ti/SiO_2$ MSSACs at various thicknesses of $SiO_2$ AR layer. ....	122
Figure 5.3	Variation of solar absorptance and thermal emittance of $SS_M/Ti/AlN/Ti/SiO_2$ MSSACs at different thicknesses of $SiO_2$ AR layer. ....	122
Figure 5.4	Variation of $n$ and $k$ for $SS_M/Ti/AlN/Ti/SiO_2$ MSSACs at different thickness of $SiO_2$ AR layer. ....	124

Figure 5.5	Cross-sectional FESEM images of Ti/AlN/Ti/SiO <sub>2</sub> MSSACs at: (a) 50 nm, (b) 80 nm, (c) 100 nm, and (d) 150 nm deposited on Si substrate at different thicknesses of SiO <sub>2</sub> .....	125
Figure 5.6	FESEM image of SS <sub>M</sub> /Ti/AlN/Ti/SiO <sub>2</sub> MSSACs at: (a) 50 nm, (b) 80 nm, (c) 100 nm, and (d) 150 nm different thicknesses of SiO <sub>2</sub> ...	126
Figure 5.7	Variation of grain size for various thicknesses of SiO <sub>2</sub> in SS <sub>M</sub> /Ti/AlN/Ti/SiO <sub>2</sub> stack. ....	126
Figure 5.8	EDX spectra of SS <sub>M</sub> /Ti/AlN/Ti/SiO <sub>2</sub> MSSACs at different thicknesses of SiO <sub>2</sub> (a) 50 nm, (b) 80 nm, (c) 100 nm, and (d) 150 nm.....	128
Figure 5.9	EDX analysis of SS <sub>M</sub> /Ti/AlN/Ti/SiO <sub>2</sub> MSSACs at different thicknesses of SiO <sub>2</sub> .....	128
Figure 5.10	3D AFM images of SS <sub>M</sub> /Ti/AlN/Ti/SiO <sub>2</sub> MSSACs at different thicknesses of SiO <sub>2</sub> (a) 50 nm, (b) 80 nm, (c) 100 nm, and (d) 150 nm.....	130
Figure 5.11	Surface roughness of SS <sub>M</sub> /Ti/AlN/Ti/SiO <sub>2</sub> MSSACs at different thicknesses of SiO <sub>2</sub> .....	130
Figure 5.12	Reflectance spectra of SS <sub>M</sub> /Ti/AlN/Ti/SiO <sub>2</sub> MSSACs annealed at different temperatures in air for 2 h. ....	132
Figure 5.13	IR reflectance spectra of SS <sub>M</sub> /Ti/AlN/Ti/SiO <sub>2</sub> MSSACs annealed at different temperatures in air for 2 h. ....	133
Figure 5.14	Variation in solar absorptance and thermal emittance with annealing temperature in air for SS <sub>M</sub> /Ti/AlN/Ti/SiO <sub>2</sub> MSSACs. ....	133
Figure 5.15	FESEM image of SS <sub>M</sub> /Ti/AlN/Ti/SiO <sub>2</sub> MSSACs annealed at different temperatures in air for 2 h. ....	134
Figure 5.16	Variation of grain size with annealing temperatures for SS <sub>M</sub> /Ti/AlN/Ti/SiO <sub>2</sub> MSSACs. ....	135
Figure 5.17	3D AFM images of SS <sub>M</sub> /Ti/AlN/Ti/SiO <sub>2</sub> MSSACs at different annealing temperatures.....	136

Figure 5.18	Variation of surface roughness as a function of annealing temperatures of $SS_M/Ti/AlN/Ti/SiO_2$ MSSACs. ....	136
Figure 5.19	XRD pattern of $SS_M/Ti/AlN/Ti/SiO_2$ MSSACs (a) as-deposited and annealed at (b) 400 °C, (c) 500 °C and (d) 600 °C in air for 2 h.....	138
Figure 5.20	Reflectance spectra of pristine, $SS_M$ substrate and the $SS_M/AlN/Ti/AlN/SiO_2$ MSSACs and annealed at different temperatures in air for 2 h. ....	139
Figure 5.21	Solar absorbance and emittance of as-deposited and annealed $SS_M/AlN/Ti/AlN/SiO_2$ MSSACs in air for 2 h. ....	140
Figure 5.22	Comparison of solar absorptance of as-deposited and annealed $SS_MTi/AlN/Ti/SiO_2$ and $SS_M/AlN/Ti/AlN/SiO_2$ MSSACs in air for 2 h.....	141
Figure 5.23	Comparison of emittance of as-deposited and annealed $SS_M/Ti/AlN/Ti/SiO_2$ and $SS_M/AlN/Ti/AlN/SiO_2$ MSSACs in air for 2 h. ....	141
Figure 5.24	FESEM micrographs of $SS_M/AlN/Ti/AlN/SiO_2$ MSSACs (a) as-deposited and annealed at (b) 400 °C, (c) 500 °C, and (d) 600 °C in air for 2 h. ....	142
Figure 5.25	3D AFM images of annealed $SS_M/AlN/Ti/AlN/SiO_2$ MSSACs annealed at various temperatures in air for 2 h. ....	143
Figure 5.26	XRD patterns of (a) as deposited $SS_M/AlN/Ti/AlN/SiO_2$ MSSACs and annealed at (b) 400 °C, (c) 500 °C and (d) 600 °C in air for 2 h.....	144
Figure 5.27	Reflectance spectra of $SS_M/Ti/AlN/Ti/SiO_2$ MSSACs before and after thermal shock test at different cycling times. ....	146
Figure 5.28	IR reflectance spectra of $SS_M/Ti/AlN/Ti/SiO_2$ MSSACs before and after thermal shock test at different cycling test times.....	147
Figure 5.29	Absorptance and emittance of $SS_M/Ti/AlN/Ti/SiO_2$ MSSACs before and after thermal shock test at different cycling times. ....	147

Figure 5.30	FESEM images of SS <sub>M</sub> /Ti/AlN/Ti/SiO <sub>2</sub> MSSACs before and after RHCC and humidity test at different cycling times: (a) 500 °C, (b) 9 cycles, (c) 15 cycles, and (d) 24 cycles.....	150
Figure 5.31	Variation of grain size with number of cycling times for SS <sub>M</sub> /Ti/AlN/Ti/SiO <sub>2</sub> MSSACs.....	150
Figure 5.32	3D AFM images of SS <sub>M</sub> /Ti/AlN/Ti/SiO <sub>2</sub> MSSACs before and after RHCC and humidity tests: (a) 500 °C, (b) 9 cycles, (c) 15 cycles, and (d) 24 cycles. ....	152
Figure 5.33	Average surface roughness of SS <sub>M</sub> /Ti/AlN/Ti/SiO <sub>2</sub> MSSACs before and after RHCC and humidity tests.....	152
Figure 5.34	Microscopic view and mean scratch width under 0.5 kgf loading condition on (A) pristine SS, (B) SS <sub>M</sub> , (C) as-deposited SS <sub>M</sub> /Ti/AlN/Ti/SiO <sub>2</sub> (D) annealed at 500 °C, and (E) after durability test.....	155
Figure 5.35	Microscopic view and mean scratch width under 1 kgf loading condition on (A') pristine SS, (B') SS <sub>M</sub> , (C') as-deposited SS <sub>M</sub> /Ti/AlN/Ti/SiO <sub>2</sub> (D') annealed at 500 °C, and (E') after durability test.....	156
Figure 5.36	Comparison of the mean scratch width of different samples under 0.5 kgf and 1 kgf loading conditions (AA'=pristine SS, BB'=SS <sub>M</sub> , CC'=as-deposited, DD'=annealed at 500 °C, and EE'=after RHCC). .....	157
Figure 5.37	IR images showing temperature at the center (∅) for LED fixed on: (a) pristine and (b) SS <sub>M</sub> , (c) SS <sub>M</sub> /Ti, (d) SS <sub>M</sub> /Ti/AlN, (e) SS <sub>M</sub> /Ti/AlN/Ti and (f) SS <sub>M</sub> /Ti/AlN/Ti/SiO <sub>2</sub> at 500 mA driven current and 30 minutes burning time. ....	159
Figure 5.38	Summary of IR surface temperatures from the back side of LED package mounted on different stack boundary configuration conditions using 500 mA for 0, 5, 10, 15, 20, 25 and 30 minutes burning time. ....	160

## LIST OF SYMBOLS

$a, c$	Lattice constants
$c$	speed of light
$D$	Crystallite size
$D_s$	Scratch depth
$d$	Interplanar distance
$h$	Plank's constant
$\alpha$	Absorptance
$\varepsilon$	Emittance
$\alpha/\varepsilon$	Selectivity
$\varepsilon_A$	Dielectric function of metal type A
$\varepsilon_B$	Dielectric function of metal type B
$\varepsilon^{MG}$	Dielectric functions in Maxwell-Gernett
$\varepsilon^{BR}$	Dielectric functions in Bruggeman
$E_b(\lambda)$	Spectrum of black body
$F_N$	Applied force
$f_A$	Filling factor
$G_\lambda$	Incident solar radiation
$G_{abs}$	Absorbed radiation
$H_s$	Scratch hardness
$hkl$	Miller indices
$k$	Extinction coefficient
$k_B$	Boltzmann's constant
$n$	Refractive index
$R_q$	Roughness
$R_h$	Maximum hill

$R_v$	Maximum valley
$r_d$	Diameter of indenter
$T_s$	Surface temperature
$W$	Scratch width
$\lambda_1$	Minimum wavelength
$\lambda_2$	Maximum wavelength
$\lambda$	Wavelength
$\theta$	Angle
%	Percentage

## LIST OF ABBREVIATIONS

AES	Auger Electron Spectroscopy
AR	Antireflection
AFM	Atomic Force Microscopy
BR	Bruggeman
CSP	Concentrating Solar Power
CVD	Chemical Vapor Deposition
DMD	Dielectric-Metal-Dielectric
DC	Direct Current
DI	Deionized
DIBAD	Dual Ion Beam Assisted Deposition
EDS	Energy Dispersive X-ray Spectroscopy
FESEM	Field Emission Scanning Electron Microscopy
FTIR	Fourier Transform Infrared Spectroscopy
FWHM	Full Width at Half Maximum
HMVF	High Metal Volume Fraction
HEAN	High Entropy Alloy Nitride
ICDD	International Centre for Diffraction Data
ICSD	Inorganic Crystal Structure Database
IBICVD	Ion-Beam Induced Chemical Vapor Deposition
IEA	International Energy Agency
IR	Infrared
LMVF	Low Metal Volume Fraction
LED	Light Emitting Diode
MG	Maxwell-Gernett
MBE	Molecular Beam Epitaxy

MDM	Metal-Dielectric-Metal
MSSAC	Multilayer Selective Solar Absorber Coating
PVD	Physical Vapor Deposition
PLD	Pulsed Laser Deposition
PEALD	Plasma Enhanced Atomic Layer Deposition
PECVD	Plasma Enhanced Chemical Vapor Deposition
PC	Performance Criterion
RMS	Root Mean Square
R	Reflectance
RF	Radio Frequency
RCA	Radio Corporation America
RHCC	Rapid Heating-Cooling Cycling
SEM	Scanning Electron Microscope
SHC	Solar Heating and Cooling
SS	Stainless Steel
SS <sub>M</sub>	Modified Stainless Steel
T	Transmittance
T <sub>iBL</sub>	Titanium bottom layer
T <sub>iTL</sub>	Titanium top layer
UV-Vis-NIR	Ultraviolet-Visible-Near Infrared
XPS	X-ray Photoelectron Spectroscopy
XRD	X-ray Diffractometer
3D	Three Dimension

## LIST OF APPENDICES

- Appendix A Basic properties of AlN
- Appendix B Basic properties of SiO<sub>2</sub>
- Appendix C Basic Properties of Ti
- Appendix D IR images showing surface temperature ( $T_s$ ) profile viewed from the rear side for LED fixed on pristine SS substrate and run at 500 mA, for (a) 0 minute, (b) 5 minutes, (c) 10 minutes, (d) 15 minutes, (e) 20 minutes, (f) 25 minutes and (g) 30 minutes burning time
- Appendix E IR images showing surface temperature ( $T_s$ ) profile viewed from the rear side for LED fixed on SS<sub>M</sub> substrate and run at 500 mA, for (a) 0 minute, (b) 5 minutes, (c) 10 minutes, (d) 15 minutes, (e) 20 minutes, (f) 25 minutes and (g) 30 minutes burning time
- Appendix F IR images showing surface temperature ( $T_s$ ) profile viewed from the rear side for LED fixed on Ti coated SS<sub>M</sub> substrate and run AT 500 mA, for (a) 0 minute, (b) 5 minutes, (c) 10 minutes, (d) 15 minutes, (e) 20 minutes, (f) 25 minutes and (g) 30 minutes burning time
- Appendix G IR images showing surface temperature ( $T_s$ ) profile viewed from the rear side for LED fixed on Ti/AlN coated SS<sub>M</sub> substrate and run at 500 mA, for (a) 0 minute, (b) 5 minutes, (c) 10 minutes, (d) 15 minutes, (e) 20 minutes, (f) 25 minutes and (g) 30 minutes burning time
- Appendix H IR images showing surface temperature ( $T_s$ ) profile viewed from the rear side for LED fixed on Ti/AlN/Ti coated SS<sub>M</sub> substrate and run at 500 mA, for (a) 0 minute, (b) 5 minutes, (c) 10 minutes, (d) 15 minutes, (e) 20 minutes, (f) 25 minutes and (g) 30 minutes burning time
- Appendix I IR images showing surface temperature ( $T_s$ ) profile viewed from the rear side for LED fixed on Ti/AlN/Ti/SiO<sub>2</sub> coated SS<sub>M</sub> substrate and run at 500 mA, for (a) 0 minute, (b) 5 minutes, (c) 10 minutes, (d) 15 minutes, (e) 20 minutes, (f) 25 minutes and (g) 30 minutes burning time

# **PENYERAP SALUTAN Ti/AlN/Ti/SiO<sub>2</sub> PELBAGAI-LAPIS NANOSKALA BAGI PERANTI SURIA TERMA**

## **ABSTRAK**

Banyak penyelidikan telah dijalankan dalam membangunkan salutan penyerap untuk aplikasi terma suria bersuhu tinggi. Namun, ketebalan yang tinggi masih menjadi isu yang serius kerana ia membawa kepada pancaran dan pengelupasan yang tinggi disebabkan oleh lekatan yang lemah pada suhu tinggi yang membawa kepada prestasi yang rendah. Dalam kerja penyelidikan ini, salutan penyerap suria berbilang lapisan Ti/AlN/Ti/SiO<sub>2</sub> telah dienapkan pada substrat keluli tahan karat (SS 316L) menggunakan magnetron sputtering Arus Terus/Frekuensi Radio (DC/RF) untuk aplikasi penyerap suria suhu tinggi. Sasaran ketulenan tinggi (99.99%) Ti, AlN dan SiO<sub>2</sub> telah digunakan. Untuk meningkatkan penyerapan suria, substrat telah diubah suai dengan penyepuhlindungan mudah di udara pada 600 °C selama 1 jam dan telah memperoleh lapisan Fe<sub>3</sub>O<sub>4</sub> pada permukaan substrat terlibat. Lapisan bawah Ti (Ti<sub>BL</sub>) kemudiannya dioptimumkan dengan mengenakan pelbagai ketebalan pada SS (SS<sub>M</sub>) yang diubah suai dan juga substrat asli. Pada ketebalan yang sama, substrat SS<sub>M</sub> dan SS asli mempamerkan penyerapan solar 64.2 dan 55.05 masing-masing. Atas dasar ini, SS<sub>M</sub> telah dipilih dan digunakan untuk keseluruhan kajian. Peningkatan yang ketara dalam penyerapan sebanyak 73.73 telah dicapai selepas mengoptimumkan lapisan AlN. Selepas mengenakan lapisan atas Ti (Ti<sub>TL</sub>), kestabilan terma yang tinggi pada 500 °C di udara selama 2 jam direkodkan dengan penyerapan suria dan pancaran haba masing-masing sebanyak 89.6 dan 19. Analisis struktur menggunakan XRD mengesahkan kehadiran kedua-dua Fe<sub>3</sub>O<sub>4</sub>, Ti dan AlN. Analisis FESEM dan AFM mendedahkan taburan seragam butiran dengan diameter ~ 47.25 nm dan kekasaran ~

73.67 nm. Penyerapan suria menurun daripada 89.6 kepada 79.1 selepas penyepuhlindapan pada 600 °C, disebabkan oleh peningkatan pantulan permukaan kerana terdapat penurunan kekasaran daripada 73.67 nm kepada 51.35 nm. Peningkatan dalam penyerapan suria sebanyak 96.90 telah dicapai selepas mengenakan lapisan antipantulan SiO<sub>2</sub>. Imej keratan rentas mendedahkan bahawa salutan terdiri daripada empat lapisan Ti/AlN/Ti/SiO<sub>2</sub>. Ujian ketahanan pada (-50 °C dan +150 °C) dan (50 °C dan 90 mmHg) ambien mendedahkan sifat optik yang stabil dan struktur mikro pada salutan tersebut. Ujian calar (mekanikal)/lekatan mendedahkan bahawa lekatan salutan bertambah baik selepas penyepuhlindapan dan ujian RHCC. Profil pemindahan haba dalam satah mendedahkan bahawa substrat SS<sub>M</sub> bersalut Ti/AlN/Ti/SiO<sub>2</sub> memaparkan profil pengagihan haba sebanyak 93.1 °C pada 500 mA, 9 V dan 30 minit masa pembakaran berbanding substrat asli dan SS<sub>M</sub>. Secara keseluruhannya, SS<sub>M</sub> bersalut Ti/AlN/Ti/SiO<sub>2</sub> mempunyai potensi aplikasi dalam penyerap suria suhu tinggi kerana penyerapan suria yang tinggi, kestabilan terma dan ketahanan yang baik dipamerkan dalam ambien yang melampau.

# NANOSCALE BASED Ti/AlN/Ti/SiO<sub>2</sub> MULTI-LAYER ABSORBER COATINGS FOR SOLAR THERMAL DEVICES

## ABSTRACT

A lot of research has been carried out in developing absorber coatings for high temperature solar thermal applications. Yet, high thickness remains serious issue as it leads to high emittance and peel due to poor adhesion at higher temperatures leading to low performance. In this research work, Ti/AlN/Ti/SiO<sub>2</sub> multilayer solar absorber coating was deposited onto stainless steel (SS 316L) substrate using Direct Current/Radio Frequency (DC/RF) magnetron sputtering for high temperature solar absorber applications. High purity (99.99%) targets of Ti, AlN and SiO<sub>2</sub> were used. To enhance solar absorption, the substrate was modified by simple annealing in air at 600 °C for 1 h and achieved Fe<sub>3</sub>O<sub>4</sub> layer on the surface of the substrate. The Ti bottom layer (Ti<sub>BL</sub>) was then optimized by depositing various thicknesses onto the modified SS (SS<sub>M</sub>) and the pristine substrates. At the same thickness, the SS<sub>M</sub> and pristine SS substrates exhibits solar absorptance of 64.2 and 55.05 respectively. On this basis, SS<sub>M</sub> was chosen and used for the rest of the study. A considerable increase in absorptance of 73.73 was achieved after optimizing AlN layer. After depositing the Ti top layer (Ti<sub>TL</sub>), a high thermal stability at 500 °C in air for 2 h was recorded with solar absorptance and thermal emittance of 89.6 and 19 respectively. Structural analysis by XRD confirms the presence of both Fe<sub>3</sub>O<sub>4</sub>, Ti and AlN. FESEM and AFM analysis revealed uniform distribution of grains with diameter of ~47.25 nm and roughness of ~73.67 nm. Solar absorptance decreased from 89.6 to 79.1 after annealing at 600 °C, due to increase in surface reflection because of decrease in roughness from 73.67 nm to 51.35 nm. An improvement in solar absorptance of 96.90 was achieved after

depositing antireflection layer of SiO<sub>2</sub>. Cross-sectional image revealed that the coating consists of four layers of Ti/AlN/Ti/SiO<sub>2</sub>. Durability test under (-50 °C and +150 °C) and (50 °C and 90 mmHg) ambient revealed the stable optical properties and microstructure of the coating. The scratch (mechanical)/adhesion test revealed that the coating's adhesion improved after annealing and RHCC test. In-plane heat transfer profile revealed that Ti/AlN/Ti/SiO<sub>2</sub> coated SS<sub>M</sub> substrate displayed heat distribution profile of 93.1 °C at 500 mA, 9 V and 30 minutes burning time compared to pristine and SS<sub>M</sub> substrates. Overall, Ti/AlN/Ti/SiO<sub>2</sub>, coated SS<sub>M</sub> has potentials application in high temperature solar absorber owing to its high solar absorption, thermal stability and good durability exhibited in harsh ambient.

# CHAPTER 1

## INTRODUCTION

### 1.1 Introduction to Solar Energy

It is generally accepted that the world's energy demand is continuously increasing because of the population explosion, industrial revolution, and technological advancement. According to basis points (bp) statistical review of world energy 2020, as of 2019, 84% of the world's primary energy consumption is generated from fossil fuel based conventional energy sources, such as petroleum, natural gas and coal [1]. The disadvantage of these fuel options is enormous such as they are not sustainable, costly and they deplete over time [2]. In addition to that, fossil fuels represent the major contributors of carbon dioxide (CO<sub>2</sub>) emissions, nitrogen oxide (NO), particulate matter, sulphur dioxide (SO<sub>2</sub>), chlorofluorocarbons (CFCs) etc. These emissions have negative impacts on the environment mainly through global warming, acidification of water cycle, decreasing air quality and overheating the earth's surface. This negative impacts of fossil fuel raised a serious environmental concerns by the world [3]. All levels of fossil fuel usage ranging from generation to storage and the end use have serious negative impacts on the environment. Therefore, an urgent need to shift from the conventional energy sources to renewable energy is necessary to avert the greenhouse gases and particulate emissions, thereby reducing extreme negative impacts of these emissions on the environment and ensuring cost effective and reliable energy delivery. As a clean, green, environmentally friendly, and renewable energy source, solar energy is abundantly distributed in almost all over the planet earth and is also the largest accessible carbon-free energy source which can be used as an alternative energy source with the help of matured technologies to replace the fossil fuel used for energy generation. The amount of solar radiation received by

the earth in the form of electromagnetic radiation on daily basis is almost 4000 trillion kWh which is about hundred times the total energy required by the world annually [4]. This energy sustains life on the earth, and it is the source of all forms of energy used by human beings. If properly harnessed, theoretically solar energy can provide more than 3000 times the present world energy demand [5]. Figure 1.1 shows the capability of the world renewable energy sources to provide more than 3000 times the present world energy needs.

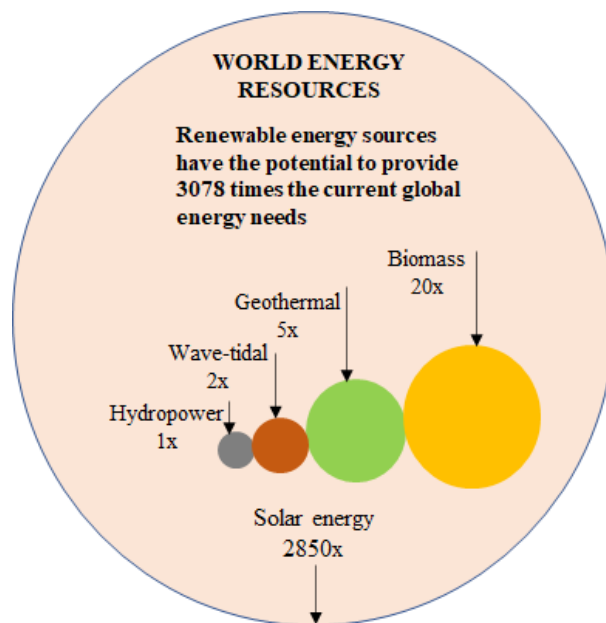


Figure 1.1 World energy resources [5].

One of the ways to harness the solar energy resources, solar thermal technologies can be employed to harness this abundant solar energy resources. In recent times, solar thermal system attracted great attention due to low financial and technical risk and simplicity in the manufacturing process [6]. Concentrating solar power (CSP) systems is the most popular among thermal technologies and is the right candidate for this purpose. Basically, locations with high sun exposure and low cloud cover are usually suitable for CSP applications. CSP is based on the principle of concentration of photons energy that come directly from the sun. the primary source

of energy for CSPs is direct normal irradiance which is mostly available in subtropical regions. CSPs have recently received great attention within the solar thermal community and become prominent in the field of power generation due to its ability to produce low cost and clean energy. CSP technology is presently deployed all over the world [3, 7] and it has the potentials for future energy generation. Although utility-scale CSP plants were in operation long before solar photovoltaics became widely commercialized, solar photovoltaics have largely taken over this market, due to their declining costs. Global CSP capacity grew only 1.6 percent in 2020 to 6.2 GW [8]. According to International Energy Agency (IEA) available technology roadmap, by 2050, CSPs could provide 11.3% of the global electricity [9].

Tabor and Gier-Dunkle was the first set of people to show the practical prospect of solar selective absorbing surfaces during the first international solar energy conference held 1955 at Tucson [10]. Since then, there was no much research on selective surfaces until when the oil crisis started in the mid-70s [11]. After which, a lot of works have been carried out on the development of absorber coatings for applications in low, mid, and high temperature solar thermal devices where high temperature coatings is now the focus for most of the present research. To increase the efficiency of CSPs, the system needs spectrally selective absorber surface with high solar absorptance ( $\alpha \geq 90$ ) in the solar range (300-2500 nm) and low thermal emittance ( $\epsilon \leq 10$ ) in the infrared (IR) range (2500-25000 nm) of solar spectrum [11, 12] at an elevated working temperature beyond 400 °C [13 – 16]. To achieve this, therefore, requires materials with stable optical properties at higher temperatures such as aluminium nitride (AlN), silicon dioxide (SiO<sub>2</sub>) and titanium (Ti).

## 1.2 Properties of AlN, SiO<sub>2</sub> and Ti

AlN is a wide band gap dielectric material whose band gap is 6.2 eV in its wurtzite form [17, 18]. AlN have recently received a great attention in the past due to its outstanding properties such as high thermal conductivity (320 W/m·K), low coefficient of thermal expansion ( $4.726 \times 10^{-6}/\text{K}$  at 500 °C), as well as high resistant to chemical attack and corrosion. Furthermore, good thermal stability of AlN at elevated temperatures makes it attractive in the field of solar absorber applications. Besides that, AlN find its great applications in piezoelectric and electronic packaging due to its high thermal conductivity [19, 20]. AlN in its wurtzite phase possess hexagonal structure with lattice constants  $a=3.112 \text{ \AA}$ , and  $c=4.982 \text{ \AA}$  [21, 22]. Each of the Al atom in the structure is surrounded by four N atoms and thus forming a tetrahedral bond.

Silicon dioxide (known as silica) is an oxide of silicon and is mostly found in nature as crystals in the form of quartz, cristobalite and tridymite [23, 24] though it is best well known as in amorphous form [26]. SiO<sub>2</sub> is known to have low refractive index, high hardness (7.0 Mohs) [27] and excellent mechanical and thermal stability [28]. These properties make it suitable for many applications. For solar thermal applications, the small value of refractive index and the high thermal stability makes it attractive candidate as an antireflection layer. This is because the low refractive index value (1.5) allows for incident light to penetrate the main active (absorbing) layers and suppress the reflected light thereby increasing the overall photothermal performance. In the structure of SiO<sub>2</sub>, each Si atom is linked tetrahedrally with four oxygen atoms in which each of the oxygen atom acts as a bridge linking the two tetrahedra [29].

Titanium is one of the transition metals found in group IV of the periodic table. It is an allotropic element which can exists in more than one crystallographic form.

Titanium finds its applications in solar thermal industries due to its outstanding properties such as high hardness (43.0 GPa), excellent thermal stability at high temperatures (1650-1670 °C), good resistant to oxidation and corrosion makes is attractive candidate as IR reflector in solar selective absorber coatings. The basic properties of these materials can be found in appendices A to C.

### **1.3 Selective Solar Absorber Coatings**

The revolution in solar thermal industry has attracted great interest into the research area of thin film solar selective absorber coatings over many decades where a clear advantage has been offered compared to the conventional paints. A lot of innovations in thin film absorber coatings have made solar thermal industry one of the leading technologies in the field of renewable solar energy harvesting. A good solar selective absorber coating is expected to absorb maximum incident solar radiation by suppressing reflection between wavelength 0.3  $\mu\text{m}$  – 2.5  $\mu\text{m}$  while maintaining low emittance at the IR region by reflecting high at a wavelength above 2.5  $\mu\text{m}$ . Achievements of high solar absorptance and low thermal emittance by different research groups [29 – 34] proved that thin film absorber coatings are the excellent candidate as coating materials that make solar thermal technologies to be a good driver for future power generation thereby phasing out the conventional fossil fuels.

Although selective absorber coatings have shown the potentials towards making solar thermal technologies as a substitute for fossil fuels in power generation, high thickness (in microns) remains an issue because it increases emittance due to IR absorption [12]. Absorber coatings with high thickness could increase the overall cost of the CSP systems due to high material consumption. High thickness could also lead to huge emittance (>20) at an elevated working temperature, and in extreme cases

could lead to delamination of the coating from the substrate or between the coated layers in the case of multilayer coatings [36]. Furthermore, thermal stability in air is also an issue. Even though several absorber coatings have shown good thermal stability above 400 °C in vacuum [36 – 39], it is also of great importance for absorber coating to be thermally stable in air in the event the vacuum is breached [11, 40]. The inability of the absorber coatings to transfer most of the absorbed solar radiation to the working fluid also affects the photothermal conversion efficiency of the CSPs. Because of the issues highlighted above, various absorber coatings have been developed by different researchers using different material combinations, sequence of stackings and synthesis routes.

#### **1.4 Theoretical Background of Spectral Selectivity**

Spectral selectivity ( $\alpha/\varepsilon$ ) of solar absorber coatings is defined as the ratio of solar radiation absorbed by the surface ( $\alpha$ ) to thermal emittance ( $\varepsilon$ ). Selectivity remains the principal focus in every solar thermal industry. This is because, selectivity determines and guarantee the photothermal efficiency of the CSP systems. Achieving selectivity entails striking a balance by minimizing reflectance in the solar region (typically 300-2500 nm) on the one hand so that to have a maximum solar absorptance and having high reflectance on the other hand at the infrared (IR) region (above 2500 nm) of solar spectrum to achieve minimum thermal emittance at the targeted operating temperature. An ideal spectrally solar selective absorber coatings should have 100% solar absorptance and 0% emittance in the solar and IR wavelength range respectively at high operating temperatures ( $T \geq 400$  °C) [42]. To achieve good spectral selectivity, several approaches were adopted by different researchers [43–46]. Some of these approaches but not limited to material selection, material combination, modification

of the substrate, optimization of synthesis parameters, multilayer coatings, and sequence of arrangement of layers. Figure 1.2 showed the ideal selective reflectance spectrum with a reference standard AM 1.5G solar irradiance and the blackbody radiation at different temperatures.

Generally, when solar radiation strikes a solid surface, three physical phenomena occur; some of the light will be reflected, some will be transmitted while some would be absorbed. The reflection, transmission and absorption depend on the wavelength of the incident light. Reflectance, ( $R$ ), is the fraction of the incident that is thrown back/reflected by a surface and it depends on the nature of the surface. The part of the incident light that passes through the material is the transmittance ( $T$ ). Absorptance, is the ratio of the incident radiation absorbed by the surface to the incident solar radiation. If  $G_{\lambda}$  represents the incident solar radiation and  $G_{abs}$  stands for the absorbed radiation, then solar absorptance can be expressed mathematically using Equation 1.1.

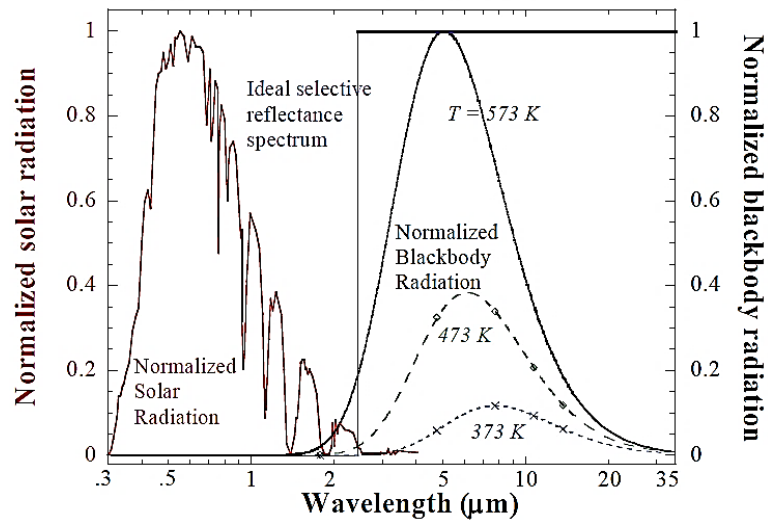


Figure 1.2 Spectral selectivity of ideal absorber coating with reference AM 1.5G solar spectrum and ideal blackbody radiation at different temperatures [47].

$$\alpha = \frac{G_{abs}(\lambda)}{G_{\lambda}(\lambda)} \quad (1.1)$$

According to conservation of energy, the total sum of the absorbed, reflected, and transmitted incident solar flux is equal to unity as expressed mathematically in Equation 1.2.

$$\alpha + R + T = 1 \quad (1.2)$$

Where  $\alpha$ ,  $R$  and  $T$  are the solar absorptance, reflectance and transmittance respectively.

In the case of an opaque substrate which do not allow for the incident solar flux to traverse through it, Equation (1.2) reduces to Equation (1.3).

$$\alpha + R = 1 \quad (1.3)$$

Where  $T$  is equal to zero. Rearranging Equation (1.3) gives

$$\alpha = 1 - R \quad (1.4)$$

The amount of solar radiation absorbed by thin film solar absorber coating can be represented in terms of reflectance using Equations (1.1) and (1.4).

$$\alpha = \frac{\int_{\lambda_1}^{\lambda_2} [1 - R] G(\lambda) d\lambda}{\int_{\lambda_1}^{\lambda_2} G(\lambda) d\lambda} \quad (1.5)$$

Where  $\lambda_1$  and  $\lambda_2$  are the minimum and maximum wavelength of the incident solar radiation of a given wavelength  $\lambda$ . Using Equation (1.5), the absorptance of a spectrally solar selective absorber coatings can be calculated using reflectance data obtained from the UV-Vis-NIR which is usually measured in the wavelength range of 300–2500 nm. This wavelength range contributes to the solar thermal applications. It is usually covers far ultraviolet (UV) (typically 300–400 nm), the whole visible range (400–700 nm) and near infrared NIR (700–2500 nm) as shown in Figure 1.3.

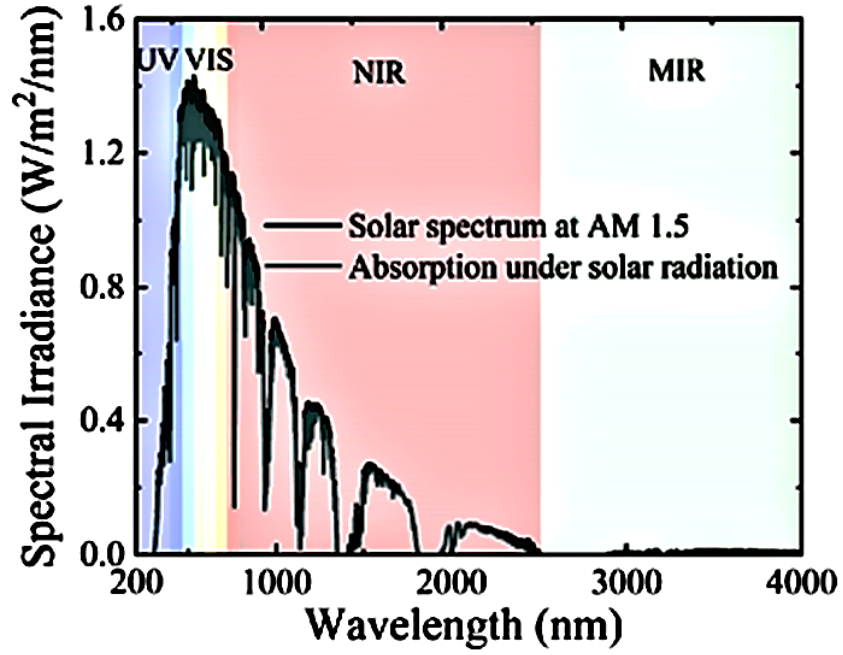


Figure 1.3 Spectrum of solar radiation [48].

Emittance,  $\varepsilon$ , is the ratio of light emitted from a surface of the coating to the perfect blackbody at equal wavelength and temperature [49]. A perfectly black body absorbs all electromagnetic radiation that is incident on it irrespective of the wavelength and emits maximum amount of energy at a given temperature. It is referred to as a perfect absorber and emitter and the distribution of this radiant energy was proposed in 1901 by Max Plank according to Equation (1.6).

$$E_{b\lambda}(\lambda, T) = \frac{8\pi hc}{\lambda^2 \exp\left(\frac{hc}{\lambda k_B T} - 1\right)} \quad (1.6)$$

Where  $c$ ,  $h$  and  $k_B$  are constants known as speed of light ( $ms^{-1}$ ), Plank's constant ( $Js$ ) and the Boltzmann's constant ( $JK^{-1}$ ) respectively.

The energy radiated from a blackbody can be estimated according to Stefan-Boltzmann law expressed in Equation (1.7).

$$E_b(T) = \int_0^{\infty} E_{b\lambda}(\lambda, T) d\lambda = \sigma T^4 \quad (1.7)$$

The law states that the energy radiated per unit area per unit time of a perfectly blackbody is proportional to the fourth power of its absolute temperature [50] where  $\sigma$  is constant. For objects other than blackbody, such as absorber coatings, the law can be further expressed as in Equation (1.8).

$$E_b(T) = \varepsilon\sigma T^4 \quad (1.8)$$

Where  $\varepsilon$  is the emissivity of the object and is equal to unity. The overall emittance can be represented by Equation (1.9).

$$\varepsilon_\lambda(T) = \frac{E_\lambda(T)}{E_b(T)} \quad (1.9)$$

Using Equation (1.4), Equation (1.9) can be rewritten in terms of emittance as follows.

$$\varepsilon_\lambda = 1 - R \quad (1.10)$$

From Equations (1.9) and (1.10) the emittance of a solar selective absorber coating at a given temperature  $T$  can be easily calculated from the IR reflectance data using Equation (1.11).

$$\varepsilon(T) = \frac{\int_{\lambda_1}^{\lambda_2} [1-R]E_b(\lambda)d\lambda}{\int_{\lambda_1}^{\lambda_2} E_b(\lambda)d\lambda} \quad (1.11)$$

Where  $E_b(\lambda)$  is the spectrum of the blackbody radiation and  $\lambda_1, \lambda_2$  are the lower and upper limit boundaries of the wavelength of interest. The emittance can be calculated from the reflectance data measured using Fourier Transform Infrared microscopy (FTIR) spectrophotometer in the wavenumber range  $400 \text{ cm}^{-1}$ - $2000 \text{ cm}^{-1}$  (5000-25000 nm).

## 1.5 Problem Statement

CSPs are the major drivers in harnessing the solar energy. Just like many other devices, application of this system depends on the progress of the coating materials used in the collector. For this reason, therefore, most collectors are coated with spectrally solar selective absorber surface. The entire photothermal performance of this collectors largely depends on the quality of the coating materials in them. However, there are several drawbacks being faced by these selective absorber surfaces some of which include:

- A lot of research has been undertaken in developing absorber coatings using dielectric-metal-dielectric (DMD) [40, 43 – 49] stack configuration compared to metal-dielectric-metal (MDM) due to high emittance associated with the metals. This issue can be addressed through modification of the substrate and using anti reflection layer of small refractive index (typically 1.5).
- Solar absorber coatings are sensitive to thickness, and it is well known that thicker coatings contribute to higher emittance due to IR absorption [12], low absorptance [57] and can lead to peel off due to poor adhesion at higher temperature. High is also thickness is not recommended for large scale industrial production as it consumes a lot of materials which will in turn increase the overall cost.
- In concentrating collectors, a pipe (typically stainless steel) which carries the working fluid is usually fixed at the focal point of the collector. These pipes are normally coated with selective absorber coatings to improve its photothermal efficiency, yet the heat distribution behaviour still not been investigated.

- So many absorber coatings exhibit high thermal stability ( $>400\text{ }^{\circ}\text{C}$ ) in vacuum [40, 58] but fails when exposed to air at higher temperature above  $400\text{ }^{\circ}\text{C}$  [39, 59] which negatively affect the photothermal conversion efficiency leading to low performance. However, stability of absorber coatings in air is paramount in case the vacuum is breached [12].
- Optical properties of absorber coatings often degrade during operation in humid and cold environments due to rapid heating-cooling cycling (RHCC) caused by either variation in season or even temperature fluctuation during time which will limits its deployment and use in cold environment.

Ti and AlN have recently received great attention in fabricating solar absorber coatings by different researchers due to their exceptional properties such as high hardness, good thermal stability at elevated temperature, resistant to oxidation, corrosion and low coefficient of thermal expansion [36]. The emissivity from the Ti can be curtail with a suitable AR layer (typically in nanometer scale). By properly optimizing the thicknesses of Ti and AlN layers, with a  $\text{SiO}_2$  as an AR layer, a reliable MDM absorber coating will be possible.

## 1.6 Objectives

- i. To grow and optimise highly efficient Ti/AlN/Ti/ $\text{SiO}_2$  based multilayer solar selective absorber coating on modified stainless steel ( $\text{SS}_M$ ) substrate.
- ii. To study and correlate the thermal stability of the optimised Ti/AlN/Ti/ $\text{SiO}_2$  MSSACs in air and in humid environment.
- iii. To characterize the adhesive behaviour of the optimised absorber coating prior and post thermal stability and durability test.

- iv. To characterize in-plane transfer profile of the absorbed heat and compare with that of the pristine and  $SS_M$  substrates.

## 1.7 Research Contribution

This research is aimed at improving the absorptance rate of solar radiation and minimizing the thermal IR radiation of absorber coatings used in concentrating solar thermal collectors. Figure 1.3 shows the absorptance and emittance magnitude of solar radiation by uncoated and coated steel pipe with solar selective absorber coating. The uncoated steel pipe absorbs the incoming solar flux partially and most of the absorbed energy is emitted as thermal radiation (Figure 1.3 (a)). As such, the temperature of the heat transfer fluid would be low due to poor absorption of the incoming solar radiation by the uncoated steel pipe. However, when the steel pipe is modified and coated with MSSAC (Ti/AlN/Ti/SiO<sub>2</sub>), there will be high absorption of incident solar radiation with little emittance. Therefore, the temperature of the working fluid will be higher than that of the uncoated one due to increased absorption of the incident solar radiation by the coating with less emittance magnitude as shown in Figure 1.3 (b). Figures 1.3 (c) and (d) depicts the schematic presentation pristine and  $SS_M$  coated with Ti/AlN/Ti/SiO<sub>2</sub> MSSAC.

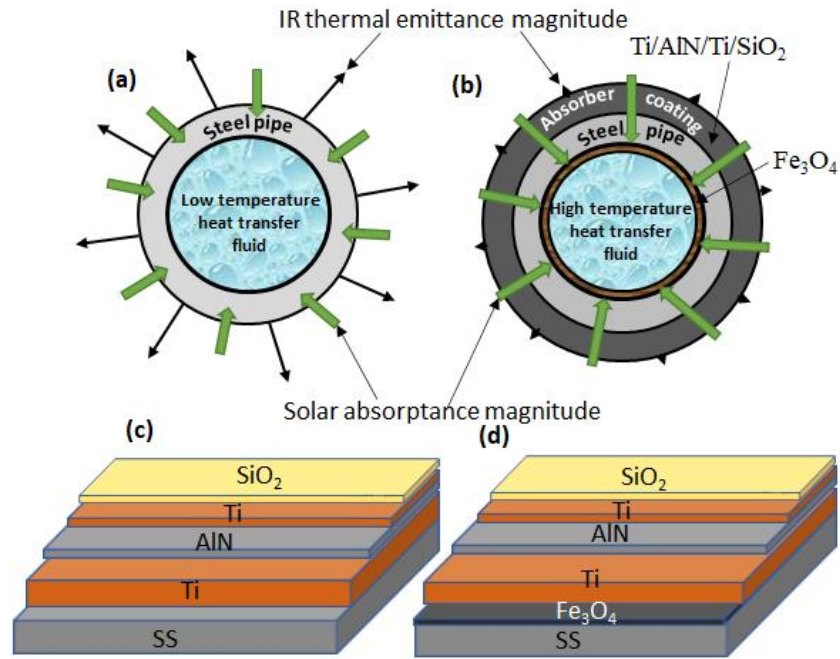


Figure 1.4 Schematic representation of cross-sectional view illustrating solar absorption and thermal IR emittance of: (a) uncoated and (b) coated steel pipes with solar selective absorber coating alongside (c) MDM coated pristine SS and (d) MDM coated SS<sub>M</sub> substrates.

A lot of solar selective absorber coatings have been developed by different researchers using different materials, different stacking arrangements on different substrates using various deposition techniques are all geared towards achieving high solar absorptance and low thermal emittance in the solar and infrared regions of solar spectrum. Recently, a lot of projects have been undertaken using DMD stack multilayer configuration as absorber coatings with a thin metal layer sandwiched between thick dielectric layers. For example, a thin Ti layer (17 nm) sandwiched between thick AlN layers of 269 nm, 51 nm and 77 nm recorded low solar absorptance of 0.88 and high thermal emittance of 0.26 [35]. High thickness (above nanometer scale) remains an issue. Therefore, we developed Ti/AlN/Ti/SiO<sub>2</sub> MSSAC with total thickness of ~185 nm compared to thick Cu/AlN/Ti/AlN/Ti/AlN with high thickness of 551 nm [35]. Similarly, Ti/AlN/Ti/SiO<sub>2</sub> deposited onto SS<sub>M</sub> exhibited solar absorptance of 0.97 compared to Mo/TiZrN/AlSiN deposited on the same SS<sub>M</sub> lower

solar absorptance of 0.95 [43]. The first time reporting of the in-plane transfer profile of the absorbed heat to the other side of the substrate [60] proved the novelty of the present work.

## **1.8 Thesis Outline**

This thesis comprises of six main chapters as follows.

**Chapter 1- Introduction:** This chapter provides the general introductory background of the availability of solar energy and the need to explore it, properties of AlN, SiO<sub>2</sub>, Ti, theoretical background spectral selectivity, solar absorber coatings, problem statement, objectives, research contribution and statement of novelty.

**Chapter 2- Literature review:** This chapter reviewed the related literature of different designs of spectrally selective absorber coatings, overview of AlN and SiO<sub>2</sub> growth techniques and the modification of SS substrate. The chapter also reviewed the nitride and oxide based solar absorber coatings and their drawbacks. Commercially available solar absorber coatings were also presented in this chapter.

**Chapter 3- Methodology:** This chapter explains the detailed methodology adopted in this study from substrates preparation, deposition of the multilayer films and the characterizations of the fabricated coatings.

**Chapter 4- Results and discussion:** This chapter discusses the optimization of Ti/AlN/Ti multilayer solar absorber coating alongside the characterizations and the analysis performed.

**Chapter 5- Optimization of SiO<sub>2</sub> AR layer:** This chapter discusses the optimization and analysis of SiO<sub>2</sub> antireflection layer on top of Ti/AlN/Ti multilayer and the effect of interchanging the layers of Ti and AlN on the solar absorptance characteristics. The chapter also discusses the thermal stability in humid and cold

environments. In-plane distribution heat distribution profile and the mechanical adhesion strength of the coating were also presented.

**Chapter 6- Summary/conclusion and recommendation:** This chapter summarizes the whole work carried out in this research project. Recommendations for future work to improve on the performance of Ti/AlN/Ti/SiO<sub>2</sub> as solar absorber coating were also given in this chapter.

## **CHAPTER 2**

### **LITERATURE REVIEW**

#### **2.1 Introduction**

This chapter seeks to offer the detail achievements in development of spectrally solar selective absorber coatings. A clear insight as regard to what has been previously done and what is expected to be done to improve the overall performance of selective absorber coatings. The chapter highlights the different absorber coatings designs adopted by various researchers towards achieving good performance. Nitride and oxide based high temperature absorber coatings with different material combination and sequence of arrangement/stacking were also reviewed and presented in this chapter. Also, various deposition techniques used in the fabrication of solar absorber coatings were highlighted. Successful commercially available mid and high temperature solar selective absorber coatings and their key properties were investigated and presented in this chapter. Finally, way forwards towards achieving excellent spectral selectivity were offered. The detailed literature used in this study has been successfully published recently [35].

#### **2.2 Different Designs of Spectrally Selective Absorber Coatings**

Spectrally solar selective absorber surfaces have gained a lot of attentions in the last decades. This has led to a numerous efforts towards fabrication of highly efficient selective absorbing coatings using different materials [3, 11, 51 – 54]. Several selective absorber surfaces have been suggested and fabricated for photothermal conversion applications [65]. From the structural perspectives, absorber coatings can be fundamentally categorised into three main types which include intrinsic absorbers, textured surface absorbers and tandem coatings. Tandem coatings are further

subdivided into four to include semiconductor-coatings, multilayer coatings, metal-dielectric composite coatings, and finally blackbody-like solar absorber coating. Solar absorber coatings can be classified into six [11, 35] types based on the different principles and structures used as represented in Figure 2.1. The schematic representations of these selective absorber types are shown in Figure 2.2.

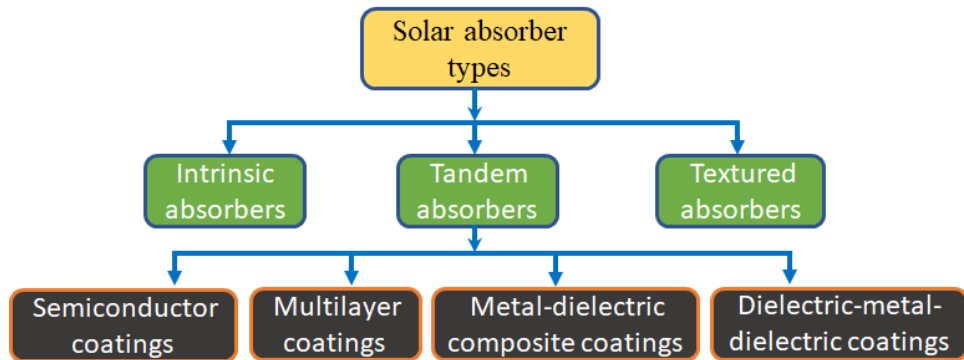


Figure 2.1 Types of selective absorber surfaces.

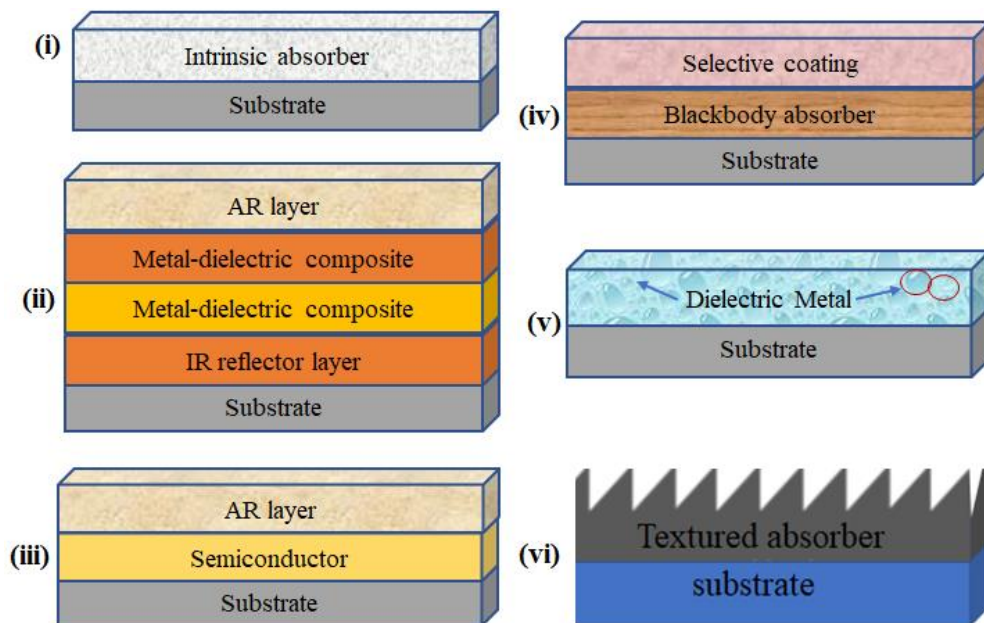


Figure 2.2 Schematic diagram of various types of solar absorber coatings (i) intrinsic absorber coating, (ii) multilayer coating, (iii) semiconductor coating, (iv) blackbody-like solar absorber coating, (v) metal-dielectric composite coating and (vi) textured surface coating.

### 2.2.1 Intrinsic absorber coatings

This type of selective absorber surfaces is structurally stable but optically inefficient unlike multilayer absorber stacks [66]. Intrinsic absorbing materials includes but not limited to; metallic tungsten (W), hafnium carbide (HfC), vanadium pentoxide ( $V_2O_5$ ), tin (IV) oxide ( $SnO_2$ ), indium oxide ( $In_2O_3$ ), molybdenum trioxide ( $MoO_3$ ) doped with molybdenum (Mo), zirconium diboride ( $ZrB_2$ ) [57, 58],  $Fe_3O_4$  [69] etc. The constituent of these materials is fundamentally derived from either lanthanide group or transition metals. Transition metals will suitably absorb solar radiation in the visible region of solar spectrum because of the presence of excess orbitals at high energy levels. When this unfilled  $d$  orbitals are combined with nitrogen, oxygen, oxynitrides and so on, they become compatible with the visible light energy [36]. In this way, intrinsic absorbers will be a potential candidate for solar thermal systems after undergoing some modifications in its properties. The intrinsic solar selective properties of W deposited at room temperature onto SS substrate using laser sintering was investigated recently [70]. The coating exhibited high solar absorptance  $\sim 0.9$  and thermal stability of up to  $650\text{ }^\circ\text{C}$ . One of the major drawback that hinders the use of most intrinsic absorbers is the occurrence of sharp step in reflectance spectra at short wavelength [3]. Moreover, for intrinsic absorbers to be able to absorb maximum incoming solar radiation, it requires high thickness of the film. Intrinsic absorbers will serve as a component of composite and multilayer coatings, but it cannot be used alone as ideal candidate for solar selective absorber coatings. This issue can only be resolved by using intrinsic materials as a dopant or to prepare composites by combining them with other materials. For example, paone et al [71] introduces W into vanadium dioxide ( $VO_2$ ) matrix as a dopant and found that it is suitable for solar thermal applications. Also, HfC requires some compositional or structural modifications in its lattice or antireflective layer to get

the required selective properties. The most commonly used antireflective layers include the following but not limited to neodymium oxide ( $\text{Nd}_2\text{O}_3$ ),  $\text{SiO}_2$ , magnesium oxide ( $\text{MgO}$ ), silicon nitride ( $\text{Si}_3\text{N}_4$ ), titanium dioxide ( $\text{TiO}_2$ ), aluminium oxide ( $\text{Al}_2\text{O}_3$ ),  $\text{ZrO}_2$ , magnesium fluoride ( $\text{MgF}_2$ ), strontium fluoride ( $\text{SrF}_2$ ), aluminium titanium oxide ( $\text{AlTiO}$ ),  $\text{AlN}$ , tantalum pentoxide ( $\text{Ta}_2\text{O}_5$ ), and titanium aluminium oxide ( $\text{TiAlO}$ ) [38, 62]. Research on intrinsic absorbers has been given less attention because it is not productive as there is no ideal intrinsic material in nature, but it is getting increasing interest as a component of multilayer absorbers.

Consider an intrinsic absorber coating as a homogeneous single thin film layer with two boundaries i.e., air-thin film and thin film- substrate boundaries, the amplitude of reflection at the two boundaries mentioned above for a normal incidence is given by Equation (2.1) and (2.2) respectively.

$$r_1 = \frac{N_o - N_1}{N_o + N_1} \quad (2.1)$$

$$r_2 = \frac{N_1 - N_2}{N_1 + N_2} \quad (2.2)$$

Where  $r_1$  and  $r_2$  represent amplitude of reflection at the air-thin film and thin film-substrate boundaries.  $N_o$ ,  $N_1$  and  $N_2$  represents the optical constants of air, thin film, and substrate respectively.

The complex part of the amplitude of reflection and the phase change can be expressed using Equations (2.3) and (2.4) respectively.

$$r = \frac{r_1 + r_2 e^{-2i\delta_1}}{r_1 + r_2 r_1 e^{-2i\delta_1}} \quad (2.3)$$

$$\delta_1 = -\frac{2\pi}{\lambda} N_1 d_1 \quad (2.4)$$

$\lambda$  and  $d_l$  are the wavelength of light and film thickness respectively. The term  $e^{-2i\delta_1}$  is referred to the phase change and is given by Equation (2.5)

$$e^{-2i\delta_1} = e^{-4\pi.k_1.d/\lambda} \cdot \left\{ \cos\left(4\pi.n_1.d/\lambda\right) + i\sin\left(4\pi.n_1.d/\lambda\right) \right\} \quad (2.5)$$

From Equation (2.5), the periodicity of sine and cosine functions which determines the interference order,  $m$ , depends on the factor  $4\pi n_1 d/\lambda$  given by Equation (2.6) [73].

$$m = 4\pi n_1 d/\lambda \quad (2.6)$$

### 2.2.2 Multilayer coatings

Figure 2.3 shows a typical multilayer structure of solar absorber coatings. By giving the optimum candidate materials, optical properties of multilayer stack can be modelled using suitable computer program [64, 65]. Higher absorptance ~95 in the visible region and low thermal IR emittance ~5 at higher temperatures can be achieved in multilayer interference stack [3] with proper optimization of the individual layer thickness. Metals such as nickel (Ni), silver (Ag), Mo and copper (Cu) and dielectric materials like CeO<sub>2</sub>, Al<sub>2</sub>O<sub>3</sub>, ZnS and SiO<sub>2</sub> have been used in high temperature multilayer absorber coatings [74]. It is worthy to mention that selecting materials with superior qualities such as low thermal expansion, optimum thermal conductivity, resistant to oxidation, high melting point and good thermal stability [36] is key towards design of high temperature multilayer coatings. For example Ti/AlN/Ti [76] and Al<sub>2</sub>O<sub>3</sub>/Mo/Al<sub>2</sub>O<sub>3</sub> [77] multilayer coatings are proved to be stable at high temperatures.

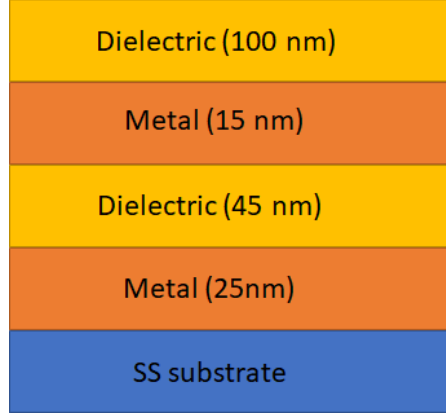


Figure 2.3 Schematic representation of multilayer interference stack.

According to Born and Wolf, 1980, reflections of light in multilayer thin film with known optical parameters can be calculated using matrix method [78]. However, summation method is more suitable for thin film with two or three layers. Therefore Equations (2.1) and (2.2) can be extended to Equation (2.7) to fit two-layer thin film having three interfaces, the amplitude reflection at the three boundaries.

$$r_3 = \frac{N_2 - N_3}{N_2 + N_3} \quad (2.7)$$

In a similar way, the phase change can be written as

$$\delta_2 = -\frac{2\pi}{\lambda} N_2 d_2 \quad (2.8)$$

Beginning from the bottom layer, that is the layer next to the substrate (for two-layer case), the sum of the reflected amplitude between 2<sup>nd</sup> and 3<sup>rd</sup> boundary can be compared with Equation (2.3) as follows.

$$r_{L2} = \frac{r_2 + r_3 e^{-2i\delta_2}}{1 + r_2 r_3 e^{-2i\delta_2}} \quad (2.9)$$

The total reflections that take place within the double layer thin film absorber coatings can be obtained by substituting  $r_2$  in Equation (2.3) with  $r_{L2}$ . This gives rise to Equation (2.10).

$$r = \frac{r_1 + r_{L2}e^{-2i\delta_1}}{1 + r_1r_{L2}e^{-2i\delta_1}} \quad (2.10)$$

In this way, Equation (2.10) can be extended for three or more layers of thin film solar absorber coatings. A suitable computer program such as MATLAB can be used to ease the calculation.

### 2.2.3 Semiconductor coatings

Semiconductor materials usually have conductivity between that of conductors (metals) and non-conductors or insulators (most ceramics). Semiconductors with band gap ranging from about ~0.5 eV (2.5 $\mu$ m) to 1.26 eV (1.0 $\mu$ m) absorb short wavelength radiation [12]. Solar radiation with energy greater than the band gap energy can be absorbed by semiconductors. When light with energy more than the energy band gap of the semiconductors is incident on a semiconductor coating, the electron in the material will be excited from valence band to the conduction band, and those with energy less than the band gap energy are transmitted.

The problem of using semiconductor materials as absorber coatings is their high refractive index value. Absorber coatings made from semiconductors will exhibit high reflectance of light from the surface due to its high index of refraction leading to poor absorptance of solar radiation and hence reduce the overall photothermal conversion efficiency. Semiconductor such as germanium (Ge), silicon (Si), lead sulphide (PbS) have been used as solar absorber coatings in the past [69 – 71]. Highly porous, thin semiconductor film structure is required as antireflecting coating for maximum transmission of light from the surface of the coating [36]. A typical AR layer (37-159 nm) like Al<sub>2</sub>O<sub>3</sub>, SiO<sub>2</sub> [15, 37, 72 – 74], Si<sub>3</sub>N<sub>4</sub> [85], etc. have been used as AR coating to curb the surface reflectance issues (<10).

#### **2.2.4 Blackbody-like solar absorber coatings**

Blackbody-like absorber coatings have the characteristics of both high absorptance and emittance. A typical ideal black body can absorb all incident solar radiation flux that strikes its surface irrespective of its wavelength or angle of incidence. Unlike other coating types, black body-like absorber coatings such as nickel oxide (NiO) doped MgO [86] will not be suitable for application as an antireflective coating due to its high emissive power tendencies. Therefore, achieving high solar absorptance and low thermal emittance in black body like absorber can be possible by depositing solar selective coating on top of it.

#### **2.2.5 Metal-dielectric composite coatings**

Metal dielectric composite also referred to as ‘cermet’ (ceramic-metal) or ‘granular’ materials are used for solar photo-thermal conversion applications. In this type of absorber coatings, fine metal particles usually from transition metals are embedded on a highly infrared reflective substrate. Optical properties of this type of absorbers can be optimized by varying the particle concentration, shape, size, orientation, and thickness of coating [35, 77]. It is recommended that the size of the cermet particles should be less than the wavelengths of light in the solar spectral range so that to enhance solar absorptance rather than scattering of the solar energy. These types of absorber coatings are strongly transparent in the infrared region and highly absorbing in the solar region (300-2500 nm) as a result of inter band transition between the metals and the small particle resonance [12] or quantum confinement also known as surface plasmon resonance (SPR) [88]. SPR is a cumulative vibration of the entire conduction electrons of the metal components within the dielectric host which enhances the optical absorption within the solar spectral range.